Atmos. Meas. Tech. Discuss., 8, 12993–13037, 2015
www.atmos-meas-tech-discuss.net/8/12993/2015/
doi:10.5194/amtd-8-12993-2015

Atmospheric Measurement Techniques Discussions

Validation of GOSAT/TANSO-FTS TIR UTLS CO_2 data (Version 1.0) using CONTRAIL measurements

N. Saitoh[1], S. Kimoto[1], R. Sugimura[1], R. Imasu[2], S. Kawakami[3], K. Shiomi[3], A. Kuze[3], T. Machida[4], Y. Sawa[5], and H. Matsueda[5]

[1]Center for Environmental Remote Sensing, Chiba University, Chiba, Japan
[2]Atmosphere and Ocean Research Institute, University of Tokyo, Kashiwa, Japan
[3]Japan Aerospace Exploration Agency, Tsukuba, Japan
[4]National Institute for Environmental Studies, Tsukuba, Japan
[5]Meteorological Research Institute, Tsukuba, Japan

Received: 15 October 2015 – Accepted: 1 December 2015 – Published: 10 December 2015

Correspondence to: N. Saitoh (nsaitoh@faculty.chiba-u.jp)

Published by Copernicus Publications on behalf of the European Geosciences Union.

Abstract

The thermal infrared (TIR) band of the Thermal and Near Infrared Sensor for Carbon Observation (TANSO)–Fourier Transform Spectrometer (FTS) on board the Greenhouse Gases Observing Satellite (GOSAT) has been observing carbon dioxide (CO_2) concentrations in several atmospheric layers since its launch. This study compared TANSO-FTS TIR V1.0 CO_2 data and CO_2 data obtained in the Comprehensive Observation Network for TRace gases by AIrLiner (CONTRAIL) project in the upper troposphere and lower stratosphere (UTLS), where the TIR band of TANSO-FTS is most sensitive to CO_2 concentrations, to validate the quality of the TIR V1.0 UTLS CO_2 data from 287 to 162 hPa. From a comparison made during flights between Tokyo and Sydney, the averages of the TIR upper atmospheric CO_2 data agreed well with the averages of the data obtained by the CONTRAIL Continuous CO_2 Measuring Experiment (CME) within 0.1 % for all of the seasons in the Southern Hemisphere. The results of a comparison for all of the eight airline routes showed that the agreement between the TIR and CONTRAIL CO_2 data was within 0.5 % on average in the Northern Hemisphere, which was better than the agreement between a priori and CONTRAIL CO_2 data. The quality of TIR lower stratospheric CO_2 data depends largely on the information content, and therefore has a seasonal dependence. In high latitudes, TIR V1.0 lower stratospheric CO_2 data are only valid in the summer. The magnitude of bias in the TIR upper atmospheric CO_2 data did not have a clear longitudinal dependence. The comparison results for flights in northern low and middle latitudes showed that the agreement between TIR and CONTRAIL CO_2 data in the upper troposphere was worse in the spring and summer than in the fall and winter. This could be attributed to a larger negative bias in the upper atmospheric a priori CO_2 data in the spring and summer and a seasonal dependence of spectral bias in TANSO-FTS TIR Level 1B (L1B) radiance data. The negative bias in northern middle latitudes made the maximum of TIR CO_2 concentrations lower than that of CONTRAIL CO_2 concentrations, which leads to underestimate the amplitude of CO_2 seasonal variation.

AMTD
8, 12993–13037, 2015

1 Introduction

Carbon dioxide (CO_2) in the atmosphere is a well-known strong greenhouse gas (IPCC, 2013, and references therein), with concentrations that have been observed both in situ and by satellite sensors. Its long-term observation began in Mauna Loa, Hawaii, and the South Pole in the late 1950s (Keeling et al., 1976a, b, 1996). Since then, comprehensive CO_2 observations in the atmosphere have been conducted worldwide in several observatories and tall towers (Bakwin et al., 1998), by aircraft flask sampling (e.g., Crevoisier et al., 2010), and via the AirCore sampling system (Karion et al., 2010) in the framework of researches by the National Oceanic and Atmospheric Administration (NOAA). Atmospheric CO_2 concentrations have gradually increased at a globally averaged annual rate of 1.7 ± 0.5 ppm from 1998 to 2011, although its growth rate has relatively large interannual variation (IPCC, 2013). Upper atmospheric CO_2 observations have been made in many areas by several projects using commercial airliners, such as the Comprehensive Observation Network for TRace gases by AIrLiner (CONTRAIL) project (Machida et al., 2008) and the Civil Aircraft for the Regular Investigation of the atmosphere Based on an Instrument Container (CARIBIC) project (Brenninkmeijer et al., 2007). Continuous long-term measurements of CO_2 made by several airplanes of Japan Airlines (JAL) in the CONTRAIL project have revealed details of its seasonal variation and interhemispheric transport in the upper atmosphere (Sawa et al., 2012) and interannual and long-term trends of its latitudinal gradients (Matsueda et al., 2015).

Atmospheric CO_2 observations by satellite sensors are categorized into two types: those utilizing CO_2 absorption bands in the shortwave infrared (SWIR) regions at around 1.6 and 2.0 µm, and those in the thermal infrared (TIR) regions at around 4.6, 10, and 15 µm. The Scanning Imaging Absorption Spectrometer for Atmospheric Chartography (SCIAMACHY) on the Environmental Satellite (ENVISAT) first observed CO_2 column-averaged dry-air mole fractions (XCO_2) from spectra at 1.57 µm (Buchwitz et al., 2005; Barkley et al., 2006). The Thermal and Near Infrared Sensor for Carbon Observation (TANSO)–Fourier Transform Spectrometer (FTS) on board the Green-

AMTD
8, 12993–13037, 2015

house Gases Observing Satellite (GOSAT), which was launched in 2009 (Yokota et al., 2009), has observed XCO_2 with high precision by utilizing the 1.6 and/or 2.0 µm CO_2 absorption bands (Yoshida et al., 2011, 2013; O'Dell et al., 2012; Butz et al., 2011; Cogan et al., 2012). The Orbiting Carbon Observatory 2 (OCO-2) was successfully launched in 2014, and started regular observations of XCO_2 with high spatial resolution. Satellite CO_2 observations at TIR absorption bands have a longer history beginning with the High-Resolution Infrared Sounder (HIRS) (Chédin et al., 2002, 2003, 2005). The Atmospheric Infrared Sounder (AIRS) has achieved more accurate observations of middle and upper tropospheric CO_2 concentrations (Crevoisier et al., 2004; Chahine et al., 2005; Maddy et al., 2008; Strow and Hannon, 2008). The Tropospheric Emission Spectrometer (TES) has retrieved CO_2 concentrations in several vertical layers with high accuracy by taking advantage of its high wavelength resolution (Kulawik et al., 2010, 2013). The Infrared Atmospheric Sounding Interferometer (IASI) has derived upper atmospheric CO_2 amounts from its TIR spectra (Crevoisier et al., 2009). TANSO-FTS also has a TIR band in addition to its three SWIR bands, and obtains vertical information of CO_2 concentrations in addition to XCO_2 in the same field of view (Saitoh et al., 2009).

Rayner and O'Brien (2001) and Pak and Prather (2001) showed the utility of global CO_2 data obtained by satellite sensors for estimating its source and sink strength, and many studies of CO_2 inversion have been conducted using a huge amount of satellite data since the 2000s. Chevallier et al. (2005) first used satellite CO_2 data, observed with the Operational Vertical Sounder (TOVS), to estimate CO_2 surface fluxes. They reported that a regional bias in satellite CO_2 data hampers the outcomes. Nassar et al. (2011) demonstrated that the wide spatial coverage of satellite CO_2 data is beneficial to CO_2 surface flux inversion through the combined use of TES and surface flask CO_2 data, particularly in regions where surface measurements are sparse. In addition to CO_2 surface inversion results using TIR observations, global XCO_2 data observed with the SWIR bands of TANSO-FTS have been actively used for estimating CO_2 source and sink strength (Maksyutov et al., 2013; Saeki et al., 2013a; Cheval-

AMTD
8, 12993–13037, 2015

lier et al., 2014; Basu et al., 2013, 2014; Takagi et al., 2014). One of the important things to consider when incorporating satellite data in CO_2 inversion is the accuracy of the data, as suggested by Basu et al. (2013). Uncertainties in satellite CO_2 data should be assessed seasonally and regionally to determine the seasonal and regional characteristics of the satellite CO_2 bias.

The importance of upper atmospheric CO_2 data in the inversion analysis of CO_2 surface fluxes was discussed in Niwa et al. (2012). They used CONTRAIL CO_2 data in conjunction with surface CO_2 data to estimate surface flux, and demonstrated that adding middle and upper tropospheric data observed by the aircraft could greatly reduce the posteriori flux errors, particularly in tropical Asian regions. Middle and upper tropospheric and lower stratospheric CO_2 concentrations and column amounts of CO_2 can be simultaneously observed in the same field of view with TANSO-FTS on board GOSAT. Provided that the quality of upper atmospheric CO_2 data simultaneously obtained with TANSO-FTS is proven to be comparable to that of TANSO-FTS XCO_2 data (Yoshida et al., 2013; Inoue et al., 2013), the combined use of upper atmospheric CO_2 and XCO_2 data observed with TANSO-FTS could be a useful tool for estimating CO_2 surface flux.

GOSAT, which is the first satellite to be dedicated to greenhouse gas monitoring, was launched on 23 January 2009. As described above, the TIR band of TANSO-FTS on board GOSAT has been observing CO_2 concentrations in several vertical layers. In this study, we focused on CO_2 concentrations in the upper troposphere and lower stratosphere (UTLS), where the TIR band of TANSO-FTS is most sensitive. We validated these data by comparison with upper atmospheric CO_2 data obtained in a wide spatial coverage in the CONTRAIL project. Sections 2 and 3 explain the GOSAT and CONTRAIL measurements, respectively. Section 4 details the retrieval algorithm used in the latest version 1.0 (V1.0) CO_2 level 2 (L2) product of the TIR band of TANSO-FTS. Sections 5 and 6 show and discuss the results of a comparison between TANSO-FTS TIR V1.0 L2 and CONTRAIL CO_2 data. Section 7 summarizes this study.

AMTD
8, 12993–13037, 2015

2 GOSAT observations

GOSAT is a joint satellite project of the National Institute for Environmental Studies (NIES), Ministry of the Environment (MOE), and Japan Aerospace Exploration Agency (JAXA) for the purpose of making global observations of greenhouse gases such as CO_2 and CH_4 (Hamazaki et al., 2005; Yokota et al., 2009). It was launched on 23 January 2009, from the Tanegashima Space Center, and has continued its observations for more than six years. GOSAT is equipped with the TANSO-FTS for greenhouse gas monitoring and the TANSO-Cloud and Aerosol Imager (CAI) to detect clouds and aerosols in the TANSO-FTS field of view (Kuze et al., 2009). TANSO-FTS consists of three bands in the SWIR region and one band in the TIR region. The SWIR bands observe column amounts of greenhouse gases and the TIR band observes vertical information of gas concentrations (Yoshida et al., 2011, 2013; Saitoh et al., 2009, 2012; Ohyama et al., 2012, 2013).

Kuze et al. (2012) provided a detailed description of the methods used for the processing and calibration of level 1B (L1B) spectral data from TANSO-FTS. They explained the algorithm for the version 150.151 (V150.151) L1B spectral data. The TIR V1.0 L2 CO_2 product we focused on in this study was created from a later version, V161.160, of L1B spectral data. The following modifications were made to the algorithm from V150.151 to V161.160: improving the TIR radiometric calibration through the improvement of calibration parameters, turning off the sampling interval non-uniformity correction, modifying the spike noise criteria of the quality flag, and reevaluating the misalignment between the GOSAT satellite and TANSO-FTS sensor. Kataoka et al. (2014) reported that the accuracies of TANSO-FTS TIR V130.130 L1B radiance spectra based on comparisons with the Scanning High-resolution Interferometer Sounder (S-HIS) spectra for warm scenes were 0.5 K at 800–900 and 700–750 cm^{-1}, 0.1 K at 980–1080 cm^{-1}, and more than 2 K at 650–700 cm^{-1}. Although the magnitude of the spectral bias evaluated on the basis of V130.130 L1B data would change in V161.160 L1B data, the issue of L1B spectral bias still remains. The spectral

AMTD
8, 12993–13037, 2015

bias inherent in TIR L1B spectra would be mainly because of uncertainty of polarization correction. Another possible cause was discussed in Imasu et al. (2010). When retrieving CO_2 concentrations from the TIR band of TANSO-FTS, the spectral bias that is predominant in CO_2 absorption bands should be considered (Ohyama et al., 2013).

3 CONTRAIL Continuous Measurement Equipment (CME) observations

We used CO_2 data obtained in the CONTRAIL project to validate the quality of TANSO-FTS TIR V1.0 L2 CO_2 data. CONTRAIL is a project to observe atmospheric trace gases such as CO_2 and CH_4 using instruments installed on commercial aircraft operated by JAL. Observations of trace gases in this project began in 2005. Two types of measurement instruments, the Automatic Air Sampling Equipment (ASE) and the Continuous CO_2 Measuring Equipment (CME), have been installed on several JAL aircraft to measure trace gases over a wide area (Machida et al., 2008).

This study used CO_2 data obtained with CME on several airline routes from Narita Airport, Japan. CO_2 observations with CME use a LI-COR LI-840 instrument that utilizes a nondispersive infrared absorption (NDIR) method (Machida et al., 2008). In the observations, two different standard gases, with CO_2 concentration of 340 and 390 ppm based on NIES09 scale, are regularly introduced into the NDIR for calibration. The accuracy of CME CO_2 measurements is 0.2 ppm. See Machida et al. (2008), Matsueda et al. (2008), and Machida et al. (2011) for details of the CME CO_2 observations and their accuracy and precision.

4 Retrieval algorithm of TANSO-FTS TIR V1.0 CO_2 data

4.1 Basic retrieval settings

Saitoh et al. (2009) provided an algorithm for retrieving CO_2 concentrations from the TIR band of TANSO-FTS. The first version, V00.01, of the L2 CO_2 product of the TIR

AMTD
8, 12993–13037, 2015

band of TANSO-FTS was basically processed by the algorithm described in Saitoh et al. (2009). The V1.0 L2 CO_2 product that we focused on in this study also adopted a non-linear maximum a posteriori (MAP) method with linear mapping, as was the case for the V00.01 product. We utilized the following expressions in TIR CO_2 retrieval:

$$\hat{\boldsymbol{z}}_{i+1} = \mathbf{W}^* \boldsymbol{x}_\mathrm{a} + \mathbf{G}\left[\boldsymbol{y} - \mathbf{F}(\hat{\boldsymbol{x}}_i) + \mathbf{K}_i \mathbf{W}\left(\mathbf{W}^* \hat{\boldsymbol{x}}_i - \mathbf{W}^* \boldsymbol{x}_\mathrm{a}\right)\right]$$
$$\mathbf{G} = \left[\mathbf{W}^T \mathbf{K}_i^T \mathbf{S}_\varepsilon^{-1} \mathbf{K}_i \mathbf{W} + \left(\mathbf{W}^* \mathbf{S}_\mathrm{a} \mathbf{W}^{*T}\right)^{-1}\right]^{-1} \mathbf{W}^T \mathbf{K}_i^T \mathbf{S}_\varepsilon^{-1} \quad (1)$$

where $\boldsymbol{x}_\mathrm{a}$ is an a priori vector, $\mathbf{S}_\mathrm{a}$ is a covariance matrix of the a priori vector, $\mathbf{S}_\varepsilon$ is a covariance matrix of measurement noise, $\mathbf{K}_i$ is a CO_2 Jacobian matrix calculated using the ith retrieval vector $\hat{\boldsymbol{x}}_i$ on full grids, $\mathbf{F}(\hat{\boldsymbol{x}}_i)$ is a forward spectrum vector based on $\hat{\boldsymbol{x}}_i$, $\boldsymbol{y}$ is a measurement spectrum vector, and $\hat{\boldsymbol{z}}_{i+1}$ is the $i+1$th retrieval vector defined on retrieval grids. $\mathbf{W}$ is a matrix that interpolates from retrieval grids onto full grids. $\mathbf{W}^*$ is the generalized inverse matrix of $\mathbf{W}$.

The full grids are vertical layer grids for radiative transfer calculation, and the retrieval grids are defined as a subset of the full grids. In the V1.0 L2 CO_2 retrieval algorithm, linear mapping between retrieval grids and full grids was also applied, but the number of full grid levels was 78 instead of 110 in the V00.01 algorithm. The determination of retrieval grids in the V1.0 algorithm basically followed the method of the V00.01 algorithm. It was based on the areas of a CO_2 averaging kernel matrix in the tropics, but the retrieval grid levels were fixed for all of the retrieval processing, as presented in Table 1. Averaging kernel matrix $\mathbf{A}$ is defined (Rodgers, 2000) as

$$\mathbf{A} = \left(\mathbf{K}^T \mathbf{S}_\varepsilon^{-1} \mathbf{K} + \mathbf{S}_\mathrm{a}^{-1}\right)^{-1} \mathbf{K}^T \mathbf{S}_\varepsilon^{-1} \mathbf{K}. \quad (2)$$

Figure 1 shows typical averaging kernel functions of TIR V1.0 L2 CO_2 retrieval in middle latitudes in summer. The degree of freedom (DF) in this case (trace of the matrix $\mathbf{A}$) was 2.09. The seasonally averaged DF values of TIR V1.0 CO_2 data ranged from 1.12 to 2.35. In the middle latitude between 35° N and 35° S, almost all the CO_2 DF

AMTD
8, 12993–13037, 2015

values exceeded 2.0; this means that observations by the TIR band of TANSO-FTS can provide information on CO_2 concentrations in more than two vertical layers, one of which we focused on in this study.

A priori and initial values for CO_2 concentrations were taken from the outputs of the NIES transport model (NIES-TM05) (Saeki et al., 2013b). A priori and initial values for temperature and water vapor were obtained from Japan Meteorological Agency (JMA) Grid Point Value (GPV) data. Basically, the retrieval processing of TANSO-FTS was only conducted under clear-sky conditions, which was judged based on a cloud flag from TANSO-CAI in the daytime (Ishida and Nakajima, 2009; Ishida et al., 2011) and on a TANSO-FTS TIR spectrum in the nighttime.

4.2 Improvements of TIR V1.0 CO_2 algorithm

The following conditions are the improvements made in the TANSO-FTS TIR V1.0 L2 CO_2 algorithm from the V00.01 algorithm. The V1.0 algorithm used the CO_2 10 µm absorption band in addition to the CO_2 absorption band at around 15 µm band; the wavelength regions of 690–750, 790–795, 930–990, and 1040–1090 cm^{-1} were used in the CO_2 retrieval. In these wavelength regions, temperature, water vapor, and ozone concentrations were retrieved simultaneously with CO_2 concentration. Moreover, surface temperature and surface emissivity were simultaneously derived as a correction parameter of the spectral bias inherent in TANSO-FTS TIR V161.160 L1B spectra at the above-mentioned CO_2 absorption bands. We assumed that the spectral bias could be divided into two components: a wavelength-dependent bias whose amount varied depending on wavelength and a wavelength-independent bias whose amount was uniform in a certain wavelength region. We tried to correct such a wavelength-independent component of the spectral bias by adjusting the value of surface temperature. Similarly, a wavelength-dependent component of the spectral bias was corrected by adjusting the value of surface emissivity in each wavelength channel. Therefore the matrices of

AMTD
8, 12993–13037, 2015

K and $\mathbf{S}_a$ of expression Eq. (1) are as follows:

$$\mathbf{K} = (\mathbf{K}_{CO_2}\mathbf{K}_{H_2O}\mathbf{K}_{O_3}\mathbf{K}_T\boldsymbol{k}_{sT\_1}\boldsymbol{k}_{sT\_2}\boldsymbol{k}_{sT\_3}\boldsymbol{k}_{sT\_4}\boldsymbol{k}_{sT\_5}\boldsymbol{k}_{sE\_1}\boldsymbol{k}_{sE\_2}\boldsymbol{k}_{sE\_3}\boldsymbol{k}_{sE\_4}\boldsymbol{k}_{sE\_5}), \quad (3)$$

$$\mathbf{S}_a = \begin{vmatrix} \mathbf{S}_{CO_2} & & & & & & & & & & & & & & \\ & \mathbf{S}_{H_2O} & & & & & & & & & & & & & \\ & & \mathbf{S}_{O_3} & & & & & & & & & & & & \\ & & & \mathbf{S}_T & & & & & & & & & & & \\ & & & & \mathbf{S}_{sT\_1} & & & & & & & & & & \\ & & & & & \mathbf{S}_{sT\_2} & & & & & & & & & \\ & & & & & & \mathbf{S}_{sT\_3} & & & & & & & & \\ & & & & & & & \mathbf{S}_{sT\_4} & & & & & & & \\ & & & & & & & & \mathbf{S}_{sT\_5} & & & & & & \\ & & & & & & & & & \mathbf{S}_{sE\_1} & & & & & \\ & & & & & & & & & & \mathbf{S}_{sE\_2} & & & & \\ & & & & & & & & & & & \mathbf{S}_{sE\_3} & & & \\ & & & & & & & & & & & & \mathbf{S}_{sE\_4} & & \\ & & & & & & & & & & & & & \mathbf{S}_{sE\_5} & \end{vmatrix}, \quad (4)$$

where $\mathbf{K}_{CO_2}$, $\mathbf{K}_{H_2O}$, $\mathbf{K}_{O_3}$, and $\mathbf{K}_T$ are Jacobian matrices of CO_2, water vapor, ozone, and temperature on full grids, respectively, and $\mathbf{S}_{CO_2}$, $\mathbf{S}_{H_2O}$, $\mathbf{S}_{O_3}$, and $\mathbf{S}_T$ are a priori covariance matrices of CO_2, water vapor, ozone, and temperature on full grids, respectively. The vectors $\boldsymbol{k}_{sT\_1}$, $\boldsymbol{k}_{sT\_2}$, $\boldsymbol{k}_{sT\_3}$, $\boldsymbol{k}_{sT\_4}$, and $\boldsymbol{k}_{sT\_5}$ are the Jacobian vectors of surface temperature in the wavelength regions of 690–715, 715–750, 790–795, 930–990, and 1040–1090 cm^{-1}, respectively. The vectors $\boldsymbol{k}_{sE\_1}$, $\boldsymbol{k}_{sE\_2}$, $\boldsymbol{k}_{sE\_3}$, $\boldsymbol{k}_{sE\_4}$, and $\boldsymbol{k}_{sE\_5}$ are the Jacobian vectors of surface emissivity in each of the five wavelength regions, respectively. The elements of the Jacobian vectors of surface parameters that were defined for each of the five wavelength regions were set to be zero in the other wavelength regions. The values $\mathbf{S}_{sT\_1}$, $\mathbf{S}_{sT\_2}$, $\mathbf{S}_{sT\_3}$, $\mathbf{S}_{sT\_4}$, and $\mathbf{S}_{sT\_5}$ and $\mathbf{S}_{sE\_1}$, $\mathbf{S}_{sE\_2}$, $\mathbf{S}_{sE\_3}$, $\mathbf{S}_{sE\_4}$, and $\mathbf{S}_{sE\_5}$ are a priori variances of surface temperature and surface emissivity in each of the five wavelength regions, respectively. Simultaneous retrieval of the surface parameters in the V1.0 algorithm was conducted just for the purpose of correcting the TIR V161.160 L1B spectral bias; it had no physical meaning. We estimated the surface parameters separately in each of the five wavelength regions to consider differences in the amount of spectral bias in each wavelength region. The matrices $\mathbf{S}_a$ for CO_2, temperature, water vapor, and ozone were diagonal matrices with vertically

AMTD
8, 12993–13037, 2015

fixed diagonal elements with a standard deviation of 2.5 %, 3 K, 20, and 30 %, respectively. Here, a priori and initial values for ozone were obtained from the climatological data for each latitude bin for each month given by MacPeters et al. (2007). We assumed rather large values as a priori variances of the surface parameters (a standard deviation of 10 K for surface temperature), which could allow more flexibility in the L1B spectral bias correction by the surface parameters. The a priori and initial values for surface emissivity were calculated on the basis of land-cover classification, vegetation, and wind speed. The a priori and initial values for surface temperature were estimated using radiance data in several channels around 900 cm^{-1} of the TIR V161.160 L1B spectra.

4.3 Effects of spectral bias on CO_2 retrieval

In the TIR V1.0 L2 algorithm, we estimated surface temperature and surface emissivity to correct the spectral bias inherent in the TANSO-FTS TIR L1B spectra (Kataoka et al., 2014). Here, we evaluated the impact of the correction of the TIR L1B spectral bias through the simultaneous retrieval of the surface parameters on the TIR L2 CO_2 retrieval. Figure 2 shows comparisons between several types of TIR CO_2 profiles retrieved by changing the treatment of the surface parameters in the retrieval and coincident CONTRAIL CME CO_2 profiles over Narita airport. Criteria for the coincident pairs of a 100 km distance from Narita airport, a time difference in 2 h, and a day difference within ±1 day yielded a total of 141 coincident profile pairs in 2010. In the comparisons, we applied averaging kernel functions of TIR CO_2 data to corresponding CONTRAIL CME CO_2 profiles, as follows (Rodgers and Connor, 2003):

$$\boldsymbol{x}_{\text{obs-CONTRAIL}} = \boldsymbol{x}_{\text{a priori}} + \mathbf{A}\left(\boldsymbol{x}_{\text{CONTRAIL}} - \boldsymbol{x}_{\text{a priori}}\right). \quad (5)$$

Here, $\boldsymbol{x}_{\text{CONTRAIL}}$ and $\boldsymbol{x}_{\text{a priori}}$ are CONTRAIL CME and a priori CO_2 profiles. Figure 2a shows a comparison of the V1.0 L2 CO_2 product (i.e., the result of a comparison of CO_2 retrievals based on TANSO-FTS TIR L1B spectra corrected through the simultaneous retrieval of both surface temperature and surface emissivity). Figure 2b and c shows

AMTD
8, 12993–13037, 2015

the results of a comparison of CO_2 retrievals that used TIR L1B spectra corrected only by surface temperature and surface emissivity, respectively. Figure 2d shows the result of a comparison of CO_2 retrievals from uncorrected original TIR L1B spectra. The existence of a relatively large spectral bias around the CO_2 15 µm absorption band in TANSO-FTS TIR L1B spectra (Kataoka et al., 2014) resulted in a decrease in the number of normally retrieved CO_2 profiles. In the V1.0 case (Fig. 2a), CO_2 profiles were normally retrieved for 74 of the 114 coincident pairs. The comparison between Fig. 2a and c (Fig. 2b and d) demonstrated that the correction of the TIR L1B spectral bias through the simultaneous retrieval of surface temperature could increase the number of normally retrieved CO_2 profiles (in this case, from 48 to 74). This implies that a wavelength-independent component of the spectral bias in CO_2 absorption bands could be reduced by adjusting the value of surface temperature at the bands. In contrast, the comparison between Fig. 2a and b (Fig. 2c and d) showed that the correction of the TIR L1B spectral bias through the simultaneous retrieval of surface emissivity had a relatively small impact on TIR L2 CO_2 retrieval. Nevertheless, surface emissivity, which has a wavelength dependence, can be effective for correcting the wavelength-dependent L1B spectral bias. A more effective method of L1B spectral bias correction based on surface emissivity should be considered in the next version of the TIR L2 CO_2 retrieval algorithm, if a future version of the TIR L1B spectral data still has a bias.

5 Comparisons of TANSO-FTS TIR V1.0 upper atmospheric CO_2 data with CME CO_2 data

5.1 Area comparisons

Here, we used the level flight CO_2 data of CONTRAIL CME observations in 2010 to validate the quality of UTLS CO_2 data from the TANSO-FTS TIR V1.0 L2 CO_2 product. The level flight data obtained in the following eight airline routes of the CONTRAIL CME observations were used in this study: Tokyo–Amsterdam (NRT–AMS) and

AMTD
8, 12993–13037, 2015

Tokyo–Moscow (NRT–DME), Tokyo–Vancouver (NRT–VYR), Tokyo–Honolulu (NRT–HNL), Tokyo–Bangkok (NRT–BKK), Tokyo–Singapore (NRT–SIN) and Tokyo–Jakarta (NRT–CGK), and Tokyo–Sydney (NRT–SYD). We merged the level flight data of Tokyo–Amsterdam and Tokyo–Moscow into "Tokyo–Europe", and the data of Tokyo–Singapore and Tokyo–Jakarta into "Tokyo–East Asia". Figure 3 shows the flight tracks of all of the CONTRAIL CME observations in 2010 used in this study. As shown in the figure, we divided the CONTRAIL CME level flight data into 40 areas following Niwa et al. (2012), and compared them with TANSO-FTS TIR CO_2 data in each area. The level flight data in each area were averaged for each season (MAM, JJA, SON, and JF/DJF). The amount of level flight data varied depending on the area and season. The largest amount was obtained in area 15 over Narita Airport, where 4694–9306 data points were obtained. A relatively small amount of level flight data, 79–222 data points, was obtained in area 1 over Amsterdam. In all 40 areas, we collected an enough amount of level flight data to undertake a comparative analysis based on the average values, except for seasons and regions with no flights. The average altitude of all of the CONTRAIL CME level flight data used here was 11.245 km. The airline routes of Tokyo–Europe, Tokyo–Vancouver, and Tokyo–Honolulu contained both tropospheric and stratospheric data in the areas along their routes; therefore, we calculated the average and standard deviation values separately. Here, we differentiated between the tropospheric and stratospheric level flight data on the basis of temperature lapse rates from the JMA GPV data that were interpolated to the CONTRAIL CME measurement locations. The average altitudes of the tropospheric and stratospheric level flight data from the airline route between Tokyo and Europe were 10.84 and 11.18 km, respectively.

Next, we selected TANSO-FTS TIR V1.0 L2 CO_2 data that were in the altitude range within ±1 km of the average altitude of the CONTRAIL level flight data for each area for each season, and calculated their averages and standard deviations. Similarly, we calculated the averages and standard deviations of the corresponding a priori CO_2 data for each area for each season. For the airline routes of Tokyo–Europe, Tokyo–Vancouver,

AMTD
8, 12993–13037, 2015

and Tokyo–Honolulu, the averages and standard deviations of TIR V1.0 CO_2 data and the corresponding a priori CO_2 data were calculated separately for the tropospheric and stratospheric data. In this calculation, we first selected TIR V1.0 CO_2 data that were collected in a range within ±1 km of the average altitudes of the CONTRAIL tropospheric and stratospheric CO_2 data for each area. Then, we classified each of the selected TIR CO_2 data points into tropospheric and stratospheric data on the basis of the temperature lapse rates from the JMA GPV data that were interpolated to the TANSO-FTS measurement locations, and calculated the seasonal averages and standard deviations for the reselected tropospheric and stratospheric TIR CO_2 data. This procedure was required for two reasons. One was that a tropopause height at each TANSO-FTS measurement location should differ on a daily basis. The other was that because TANSO-FTS TIR CO_2 data were selected within the range of 2 km, some tropospheric TIR CO_2 data were selected on the basis of the CONTRAIL stratospheric level flight data, and vice versa. Figure 4 shows the number of TANSO-FTS TIR CO_2 data points that were finally selected in each retrieval layer for each of the airline routes. The TIR CO_2 data used in the comparative analysis were from layer 9 and layer 10 (from 287 to 196 hPa) for the tropospheric comparison and from layer 10 and layer 11 (from 237 to 162 hPa) for the stratospheric comparison.

We did not apply TIR CO_2 averaging kernels to CONTRAIL CME CO_2 data in the following UTLS analysis. Because CO_2 concentrations below and above the CONTRAIL CME flight levels were not observed except over airports, assuming a CO_2 vertical profile for each of CONTRAIL CME level flight data points and applying averaging kernels to the assumed CONTRAIL CO_2 profiles would increase the uncertainty in the CONTRAIL CO_2 data. Here, we assess the effect of not applying averaging kernels to CONTRAIL CME level flight data. Figure 5a shows the means of the averaging kernels of each of the three layers 9, 10, and 11 of all of the TANSO-FTS TIR CO_2 profiles used in the comparisons in summer. In Fig. 5, we show examples of area 40 in the airline route between Tokyo and Honolulu, where we had a large amount of data for comparison, and area 1 in the airline route between Tokyo and Amsterdam, where

AMTD
8, 12993–13037, 2015

we had data for comparison both in the troposphere and stratosphere. Considering the half-value width of the averaging kernels in Fig. 5a, the TANSO-FTS TIR CO_2 retrieval results in layers 9–11 would be affected by CO_2 concentrations from ~ 400 to ~ 120–130 hPa. As shown in the CONTRAIL CME ascending/descending CO_2 profiles in Fig. 5b, the variability in the CO_2 concentration from ~ 400 to ~ 200 hPa was relatively small in summer; the same was true in the other three seasons. This indicates that CO_2 concentrations below layer 9 had a small impact on the TIR CO_2 retrieval results in layers 9 and 10, which suggests that the following results do not change much, even when considering the averaging kernels related to the layers below layer 9. Consequently, we determined not to apply TIR CO_2 averaging kernels to CONTRAIL CME CO_2 data in this study. However, because we did not have CONTRAIL CME CO_2 data above ~ 200 hPa, we could not evaluate the impact of the CO_2 concentration above ~ 200 hPa on TANSO-FTS TIR CO_2 retrieval results in layers 9–11 on the basis of observation data. Thus, we should discuss again the effect of not applying averaging kernels to CONTRAIL CME data on the following comparison results in Sect. 6.

5.2 Results of the comparisons

The airline route between Tokyo and Sydney covered a wide latitude range from the northern mid-latitudes (35° N) to southern mid-latitudes (34° S). Figure 6 shows the comparisons among CONTRAIL CME level flight, TANSO-FTS TIR, and a priori CO_2 data during flights between Tokyo and Sydney in spring. The average of the TIR CO_2 data agreed better to the average of the CONTRAIL CO_2 data than the a priori CO_2 data in all of the latitudes. In the Southern Hemisphere, the average of the TIR CO_2 data was within 0.1 % of the average of the CONTRAIL CO_2 data. In the Northern Hemisphere, the average of the TIR CO_2 data agreed with the average of the CONTRAIL CO_2 data to within 0.5 %, although their agreement became slightly worse there compared to the Southern Hemisphere.

Along the airline route between Tokyo and Europe, both tropospheric and stratospheric CO_2 data were obtained in the CONTRAIL CME observations. Therefore, we

AMTD
8, 12993–13037, 2015

were able to validate the quality of TANSO-FTS TIR CO_2 data for this route both in the upper troposphere and lower stratosphere using the UTLS CONTRAIL CO_2 data. Figure 7b and c shows that the differences between the upper tropospheric and lower stratospheric CO_2 concentrations of CONTRAIL CME data were approximately 2–3 ppm in the winter (maximum of 4.24 ppm in area 14). The upper tropospheric and lower stratospheric CO_2 concentrations from TANSO-FTS TIR V1.0 data also differed clearly, while the upper tropospheric and lower stratospheric CO_2 concentrations from a priori data were similar. The upper tropospheric CO_2 concentrations were in fairly good agreement with the corresponding CONTRAIL CME data (Fig. 7b). In the lower stratosphere in winter (Fig. 7c), the averages of the CONTRAIL CME level flight, TANSO-FTS TIR, and a priori CO_2 data were nearly identical.

Figure 8 shows the results of all of the comparisons among CONTRAIL CME, TANSO-FTS TIR, and a priori CO_2 data for each of the six (eight) airline routes for each season. The thick and dashed lines indicate the differences between CONTRAIL CME and TANSO-FTS TIR CO_2 data (TIR ave. minus CONTRAIL ave.) and the differences between CONTRAIL CME and a priori CO_2 data (a priori ave. minus CONTRAIL ave.) for each of the areas along the airline routes. All of the results with more than three data points are presented. Overall, the thick lines are closer to zero than the dashed lines, which means that TIR CO_2 data agreed better to CONTRAIL CO_2 data than a priori CO_2 data.

For the airline route between Tokyo and Europe (Fig. 8a), the agreement between tropospheric TANSO-FTS TIR and CONTRAIL CME CO_2 average data seemed slightly better in winter, although comparisons among seasons in the troposphere were difficult because of the lack of CONTRAIL CME data in high latitudes in the spring and summer (Fig. 8a1). In the stratosphere (Fig. 8a2), the averages of TIR and CONTRAIL CO_2 data agreed well with each other, and their differences were within ~ 0.5–1 ppm in the spring, summer, and winter. The differences between the two averages were slightly larger in the fall (approximately 2 ppm). For the airline route between Tokyo and Vancouver (Fig. 8b), the averages of the TIR CO_2 data were more similar to the averages of

AMTD
8, 12993–13037, 2015

the CONTRAIL CO_2 data than the a priori CO_2 data both in the upper troposphere and lower stratosphere in the fall and winter; the differences between the TIR and CONTRAIL CO_2 average data were approximately within 1 ppm. For the airline route between Tokyo and Honolulu (Fig. 8c), the agreement between TIR and CONTRAIL CO_2 average data did not show clear seasonal differences in the lower stratosphere (Fig. 8c2), because of a small number of stratospheric data. In contrast, in the upper troposphere (Fig. 8c1), the differences between the two were clearly larger in the spring and summer than in the fall and winter. In particular, both the differences between TIR and CONTRAIL CO_2 data and between a priori and CONTRAIL CO_2 data were larger in spring, as was the case for the results of the comparison for the airline route between Tokyo and Vancouver (Fig. 8b1).

Then, we focused on the results of the comparison between TANSO-FTS TIR and CONTRAIL CME upper tropospheric CO_2 data obtained in northern low and middle latitudes. Figure 8d shows that the agreement between TIR and CONTRAIL CO_2 average data was worse in the spring and summer than in the fall and winter for the airline route between Tokyo and Bangkok. The differences between TIR and CONTRAIL CO_2 data exceeded the 1-σ standard deviations of the averages of TIR CO_2 data, and were larger than the differences between a priori and CONTRAIL CO_2 data at 23–34° N (area 20) in the summer. Similarly, the agreement between the averages of TIR and CONTRAIL CO_2 data was worse in the spring and summer than in the fall and winter for the airline route between Tokyo and East Asia (Fig. 8e).

For the airline route between Tokyo and Sydney (Fig. 8f), the average of the TANSO-FTS TIR CO_2 data was within 1 ppm of the average of the CONTRAIL CME CO_2 data in the Southern Hemisphere in all of the seasons, as in the comparison in the spring shown in Fig. 6. However, in the Northern Hemisphere, the agreement between the two was not as strong in all of the seasons. In the comparisons in the northern summer, although the differences between the average TIR and CONTRAIL CO_2 data were less than 1 % (3 ppm), there was a relatively large negative bias in the TIR CO_2 data against the CONTRAIL CO_2 data compared to the other seasons. In the upper troposphere in

AMTD
8, 12993–13037, 2015

northern summer, TIR CO_2 data showed a significantly good agreement with CONTRAIL CO_2 data compared to a priori CO_2 data in the Southern Hemisphere. However, in northern low and middle latitudes, TIR and a priori CO_2 data had a negative bias of up to 1 % against CONTRAIL CO_2 data.

6 Discussion

Figure 9 shows the averages of the partial degree of freedom of TANSO-FTS TIR V1.0 L2 CO_2 data for each of the areas along the airline route between Tokyo and Europe in the upper troposphere (a) and the lower stratosphere (b) for each season. The partial DF is defined as the trace of a submatrix of averaging kernels corresponding to a partial column of TIR CO_2 data that were compared to CONTRAIL CME level flight data, which is equal to the averages of the 9th, 10th, or 11th diagonal element of matrix **A**. As shown in Fig. 9, the values of the partial DF of TIR lower stratospheric CO_2 data were clearly lower than those of TIR upper tropospheric CO_2 data for all of the fights between Tokyo and Europe. TIR upper tropospheric CO_2 data were from layers 9 and 10, and TIR lower stratospheric CO_2 data were from layers 10 and 11, as shown in Fig. 4, which led to a clear difference in partial DF values between the TIR upper tropospheric and lower stratospheric CO_2 data. The partial DF values of TIR upper tropospheric CO_2 data were 0.13–0.20 in all of the areas for all seasons. In contrast, the partial DF values of TIR lower stratospheric CO_2 data in the spring, fall, and winter were $\sim$ 0.05 in almost all of the areas, although they were as high as 0.1–0.14 in the summer. The thick lines in Fig. 8a2 show that the agreement of TIR and CONTRAIL CO_2 data in the lower stratosphere was better in the spring, summer, and winter than in the fall. The dashed lines in Fig. 8a2 also show that a priori CO_2 data agreed better with CONTRAIL CME CO_2 data in the lower stratosphere in the spring and winter than in the summer and fall. From the results shown in Fig. 8a2 and Fig. 9, we conclude that TIR CO_2 retrieval results in the lower stratosphere in the spring and winter were constrained to the relatively good a priori CO_2 data due to the low information content,

AMTD
8, 12993–13037, 2015

and consequently had a good agreement with CONTRAIL CO_2 data. In the fall, TIR CO_2 retrieval results in the lower stratosphere were constrained to the relatively poor a priori CO_2 data, and therefore had a negative bias of approximately 2 ppm against CONTRAIL CO_2 data. In the summer, TIR CO_2 retrievals had a relatively high information content compared to the other seasons, which led to a good agreement between TIR and CONTRAIL CO_2 data despite the relatively poor a priori CO_2 data. In conclusion, the quality of TIR V1.0 CO_2 data in the lower stratosphere depends largely on the information content compared to the upper troposphere. In the case of high latitude measurements, TIR V1.0 lower stratospheric CO_2 data are only valid in the summer.

As shown in Fig. 8d–f, the agreement between TANSO-FTS TIR and CONTRAIL CME CO_2 data was worse in the spring and summer than in the fall and winter in northern low and middle latitudes. At these latitudes, TIR upper tropospheric CO_2 data had a negative bias of up to ~ 1 % against CONTRAIL upper tropospheric CO_2 data. This characteristic was also seen in the data from flights between Tokyo and Honolulu where there was a large amount of upper tropospheric data available in all of the seasons (Fig. 8c1). Overall, as shown in Fig. 8, a priori CO_2 data used in TIR V1.0 CO_2 retrievals had a negative bias against CONTRAIL CO_2 data. The a priori CO_2 data in the spring and summer in Fig. 8d–f clearly had a larger negative bias against the corresponding CONTRAIL CO_2 data. The results show that a priori CO_2 data taken from NIES-TM 05 underestimate the increase in the CO_2 concentration in the upper atmosphere in spring and summer, which results in a larger negative bias of TIR V1.0 upper tropospheric CO_2 data in the spring and summer than in the fall and winter in northern low and middle latitudes.

In general, information content of CO_2 observations made by TIR sensors is higher in middle and high latitudes in the spring and summer than in the fall and winter because of thermal contrast in the atmosphere, with less seasonal dependence in low latitudes. Therefore, in the spring and summer, retrieved CO_2 data contain more measurement information and are less constrained by a priori data in all latitudes. However, as shown in Fig. 8, the retrieved TIR CO_2 data in the Northern Hemisphere did not sufficiently

AMTD
8, 12993–13037, 2015

reduce the negative bias of the a priori CO_2 data in the spring and summer. The degree of improvement in the spring and summer was comparable to or worse than in the fall and winter. This implies the existence of factors that worsened CO_2 retrieval results other than the poor a priori data in the spring and summer. One of the possible factors is uncertainty in JMA GPV temperature profiles used in TIR V1.0 L2 CO_2 retrieval. If they have some seasonal bias, seasonally dependent bias in retrieved CO_2 data would be produced. However, the TIR V1.0 algorithm simultaneously retrieved temperature profiles other than CO_2, and therefore the effect of temperature uncertainty on retrieved CO_2 data should be reduced.

Another possible factor that worsened CO_2 retrieval results is uncertainty in the calibration of TIR V161.160 L1B spectra. This means that the amount of TIR V161.160 L1B spectral bias has some seasonal dependence. Therefore, we investigated an appropriate parameter to evaluate the uncertainty in TANSO-FTS TIR L1B spectra. The temperatures of the internal blackbody on board the TANSO-FTS instrument partly reflect the environmental thermal condition inside the instrument. The temperatures of FTS-mechanics and aft-optics on the optical bench of the TANSO-FTS instrument are precisely controlled at 23 °C. The difference in temperature between the environment inside the instrument and the optical bench would cause the uncertainty in radiometric calibration of TANSO-FTS L1B spectra. Thus, the temperatures of the internal blackbody on board the TANSO-FTS instrument could be a parameter to evaluate the TANSO-FTS TIR L1B spectral bias.

Figure 10 is a scatter-plot of the average temperatures of the onboard internal blackbody and the average differences between TANSO-FTS TIR and CONTRAIL CME CO_2 data shown in Fig. 8 for each area for each season. The average temperatures of the on-board internal blackbody were lower in the spring and summer than in the fall and winter in all of the areas. It can be seen from Fig. 10 that the internal blackbody temperatures in the summer (diamonds) were lower than those in the other seasons (crosses). As discussed above, a priori CO_2 data had a larger negative bias against CONTRAIL CME CO_2 data particularly in northern low and middle latitudes in the spring and sum-

AMTD
8, 12993–13037, 2015

mer, which led to a larger negative bias in retrieved TIR CO_2 data at these latitudes. In addition, retrieved TIR CO_2 data had a larger bias in summer when the internal blackbody temperatures were lower, even if the amount of negative bias in a priori CO_2 data in summer was comparable to that in the other seasons, as shown in Fig. 10. As stated above, the temperature of the onboard internal blackbody could be a candidate for evaluating the spectral bias. At this moment, however, there is no definite evidence of a clear correlation between the temperatures of the onboard internal blackbody and the bias in TANSO-FTS V161.160 L1B spectra that would subsequently cause the seasonally dependent bias in the TIR V1.0 L2 CO_2 data, because the correlation between the average temperatures of the onboard internal blackbody and the average differences between TIR and CONTRAIL CO_2 data is not very strong.

The TANSO-FTS TIR V1.0 L2 CO_2 algorithm simultaneously retrieves surface temperature and surface emissivity as a corrective parameter of the bias in TIR L1B spectra. Therefore, the uncertainty in these surface parameters would have a large impact on retrieved TIR CO_2 profiles. Figure 7d and e in Saitoh et al. (2009) show that the uncertainty of retrieved UTLS CO_2 concentrations in layers 9–11 is much less than 1 % when the surface parameters have 1 % uncertainty, although the uncertainty of CO_2 concentrations at $\sim$ 400 hPa reaches 3 % for the same condition. We conclude that the uncertainty of the surface parameters has a relatively small impact on the TIR UTLS CO_2 concentrations that were the focus of this study. The uncertainties in surface parameters and water vapor in lower atmosphere largely affect lower and middle tropospheric TIR CO_2 data, and therefore should be discussed when validating the quality of TIR CO_2 data in the lower and middle troposphere, which is beyond the scope of this paper.

We compared TANSO-FTS TIR V1.0 L2 upper tropospheric and lower stratospheric CO_2 data that were mainly from layers 9 and 10 and from layers 10 and 11 with the corresponding CONTRAIL CME tropospheric and stratospheric CO_2 data without applying the TIR CO_2 averaging kernels to the CONTRAIL CO_2 data. As discussed above, CO_2 concentrations below layer 9 have a small impact on TIR CO_2 retrieval results in layers

AMTD
8, 12993–13037, 2015

9 and 10, because the variability in the CO_2 concentration from ~ 400 to ~ 200 hPa was relatively small in all of the seasons. However, in layer 11, TIR CO_2 retrieval results could be overestimated by the effect of the CO_2 concentration below layer 9, if the atmosphere in layer 11 is stratospheric air with relatively low CO_2 concentrations. On the other hand, TIR CO_2 retrieval results in layers 9–11 could also be affected by CO_2 concentration from ~ 200 to ~ 120–130 hPa, judging from the half-value width of the averaging kernels in Fig. 5a. If the atmosphere from ~ 200 to ~ 120–130 hPa is stratospheric air with low CO_2 concentrations, retrieved TIR CO_2 concentrations in layers 9–11 could be underestimated. In summary, retrieved TIR CO_2 concentrations could be underestimated in layers 9–10, and face the conflicting possibility of being overestimated and/or underestimated in layer 11. However, because we did not have CO_2 observation data below and above the CONTRAIL CME flight levels, we cannot reach a definite conclusion. As shown in Fig. 8, TIR upper tropospheric CO_2 data had a slightly negative bias against CONTRAIL CME CO_2 data. In the comparison of the airline route of Tokyo–Sydney as shown in Fig. 6, the differences between the averages of TIR CO_2 data and the averages of CONTAIL CO_2 data were slightly larger in the Northern Hemisphere (0.5 %) than in the Southern Hemisphere (0.1 %). The difference between upper tropospheric and lower stratospheric CO_2 concentrations is larger in the Northern Hemisphere in spring (Sawa et al., 2012), which would cause a slightly larger negative bias in the Northern Hemisphere than in the Southern Hemisphere. The effect of lower CO_2 concentrations from ~ 200 to ~ 120–130 hPa on TIR CO_2 retrieval results in layers 9–10 could be one of the causes of a negative bias in retrieved CO_2 data other than the negative bias of a priori CO_2 data and the spectral bias of TIR V161.160 L1B spectra.

We investigated differences between TIR and CONTRAIL CO_2 comparison results in layers 9–11 with and without applying averaging kernel functions although in limited areas over several airports where CO_2 vertical profiles were observed. Following the method proposed by Araki et al. (2010), we used CONTRAIL ascending/descending CO_2 data below a tropopause and stratospheric CO_2 concentrations taken from the

AMTD
8, 12993–13037, 2015

Nonhydrostatic Icosahedral Atmospheric Model (NICAM)–Transport Model (TM) (Niwa et al., 2011) to create CO_2 profiles over airports. In northern middle latitudes in the spring (over NRT airport), considering averaging kernel functions by using expression Eq. (5) decreased a negative bias in TIR CO_2 data in layers 9 and 10 by ∼ 1 ppm. On the other hand, the same tendency was not seen in southern middle latitudes in the spring (SYD) when considering averaging kernel functions. This is consistent with the above discussion related to Sawa et al. (2012). In the summer and fall in middle latitudes in both hemispheres, the effect of considering averaging kernel functions on TIR and CONTRAIL CO_2 comparison results was negligible (less than ∼ 0.5 ppm), although CONTRAIL CO_2 data in layers 9 and 10 with averaging kernel functions became slightly larger there. In low latitudes (BKK, SIN, and CGK), differences between TIR and CONTRAIL CO_2 comparison results in layers 9 and 10 with and without considering averaging kernel functions were also negligible in every season. In northern high latitudes (AMS and YVR), bias of TIR lower stratospheric CO_2 data against CONTRAIL CO_2 data in layers 10 and 11 tended to diminish when considering averaging kernel functions, and the effect of considering averaging kernel functions on TIR and CONTRAIL upper tropospheric CO_2 comparison results in layers 9 and 10 was again negligible.

Using CONTRAIL CME level flight observations that covered wide spatial areas makes us discuss a longitudinal difference in the characteristics of TIR UTLS CO_2 data. In the comparison results of the airline routes of Tokyo–Europe and Tokyo–Vancouver shown in Fig. 8a and b, the magnitudes of differences between TIR and CONTRAIL CO_2 data were similar in every longitude in the fall and winter in the upper troposphere and in every season in the lower stratosphere, although there is little logic to discuss the longitudinal differences in the spring and summer in the upper troposphere because of a small number of the data. On the other hand, in the comparison results of Tokyo–Honolulu, differences between TIR and CONTRAIL CO_2 data became larger toward ∼ 165° W (195° in Fig. 8c1) in the spring. This area is located at 25° N, and differences between TIR and CONTRAIL CO_2 data were also large in area 20 (in the airline route

AMTD
8, 12993–13037, 2015

of Tokyo–Bangkok), area 27 (Tokyo–East Asia), and area 28 (Tokyo–Sydney) located in the same latitude region, which implies that these biases depended on latitude, not on longitude. We conclude that the data quality of TIR V1.0 L2 UTLS CO_2 data does not have a clear longitudinal dependence. Finally, we evaluated bias values of TIR V1.0 CO_2 data against CONTRAIL CME CO_2 data for each season for each of the latitude regions: 60–70° N (areas 3–13), 40–60° N (areas 1, 2, 14, 35, 37, 41–43), 20–40° N (areas 15, 20, 21, 27, 28, 36, 38–40), 0–20° N (areas 18, 22, 19, 25, 26, 29, 30), 0–20° S (areas 23, 31, 32), and 20–40° S (areas 33, 34). The bias values are the weighted averages of differences between TIR and CONTRAIL averaged CO_2 data of the areas located in each latitude region with considering the number of TIR CO_2 data in each of the areas. In the upper troposphere in 20–60° N, negative biases in TIR CO_2 data ranging from 2.2 to 2.7 ppm and from 1.2 to 1.6 ppm were seen in the spring and summer, respectively, as summarized in Table 2. Although the evaluation on the basis of NICAM-TM stratospheric CO_2 concentrations in limited areas over several airports, considering averaging kernel functions decreased a negative bias in TIR CO_2 data by ∼ 1 ppm in the spring and slightly increased a negative bias in the summer in northern middle latitudes. Thus, the following negative biases should be considered when incorporating TIR V1.0 upper tropospheric CO_2 data in inverse models which usually consider averaging kernel functions: ∼ 2.0 ppm in both spring and summer in 20–40° N, ∼ 1.0 ppm in spring and ∼ 1.5 ppm in summer in 40–60° N. In northern low latitudes (0–20° N), the negative bias of 2.0 ppm should be taken into account in summer, as presented in Table 2. In the lower stratosphere in northern high latitudes, bias of TIR CO_2 data against CONTRAIL CME CO_2 data tended to diminish when considering averaging kernel functions. It is the negative biases in northern low and middle latitudes that we should mainly care about when using TIR V1.0 L2 CO_2 data in any scientific analysis. In the upper troposphere in northern middle latitudes, CO_2 concentrations reach the maximum from spring through early summer. The negative biases in TIR CO_2 data there make the maximum of TIR CO_2 concentrations lower than that of CONTRAIL CME CO_2 concentrations, which leads to underestimate the amplitude of

AMTD
8, 12993–13037, 2015

CO_2 seasonal variation when using TIR CO_2 data without taking their negative biases into account.

7 Summary

In this study, we conducted a comprehensive validation of the UTLS CO_2 concentrations from the GOSAT/TANSO-FTS TIR V1.0 L2 CO_2 product. The TIR V1.0 L2 CO_2 algorithm used both the CO_2 10 and 15 µm absorption bands (690–750, 790–795, 930–990, and 1040–1090 cm^{-1}), and simultaneously retrieved vertical profiles of CO_2, water vapor, ozone, and temperature in these wavelength regions. Because TANSO-FTS TIR V161.160 L1B radiance data used in the TIR V1.0 L2 CO_2 retrieval had a spectral bias, we simultaneously derived surface temperature and surface emissivity in the same wavelength regions just as a corrective parameter, other than temperature and gas profiles, to correct the spectral bias. The simultaneous retrieval of surface temperature greatly increased the number of normally retrieved CO_2 profiles.

To validate the quality of TIR V1.0 upper atmospheric CO_2 data, we compared them with the level flight CO_2 data of the CONTRAIL CME observations along the following airline routes in 2010: Tokyo–Europe (Amsterdam and Moscow), Tokyo–Vancouver, Tokyo–Honolulu, Tokyo–Bangkok, Tokyo–East Asia (Singapore and Jakarta), and Tokyo–Sydney. For the CONTRAIL data obtained during the northern high latitude flights, we made comparisons among CONTRAIL, TIR, and a priori CO_2 data separately in the upper troposphere and in the lower stratosphere. The TIR upper tropospheric and lower stratospheric CO_2 data that were compared were mainly from layers 9 and 10 (287–196 hPa) and from layers 10 and 11 (237–162 hPa), respectively.

In the Southern Hemisphere, the averages of TIR upper atmospheric CO_2 data were within 0.1 % of the averages of CONTRAIL CO_2 data for all of the seasons, from the limited comparisons made during flights between Tokyo and Sydney. In the Northern Hemisphere, TIR CO_2 data had a better agreement with CONTRAIL CO_2 data than a priori CO_2 data, with the agreement being on average within 0.5 %. The northern high

AMTD
8, 12993–13037, 2015

latitude comparisons suggest that the quality of TIR lower stratospheric CO_2 data depends largely on the information content. In high latitudes, TIR V1.0 lower stratospheric CO_2 data are only valid in the summer when their information content is highest. In the northern low and middle latitudes, the agreement between TIR and CONTRAIL CO_2 data in the upper troposphere was worse in the spring and summer than that in the fall and winter, partly because of a larger negative bias in the a priori CO_2 data in the spring and summer than in the fall and winter. In addition, a seasonal dependence of the spectral bias inherent to TANSO-FTS TIR L1B radiance data could cause a negative bias in retrieved CO_2 concentrations, particularly in summer. TIR sensors can make more observations than SWIR sensors. The combined use of TIR UTLS CO_2 data and XCO_2 data from the SWIR bands of TANSO-FTS can be useful for studies of CO_2 surface flux inversion and atmospheric transport, provided that the seasonally and regionally dependent negative biases of the TIR V1.0 L2 CO_2 data presented here are taken into account.

Acknowledgements. We thank all of the members of the GOSAT Science Team and their associates. We are also grateful to the engineers of Japan Airlines, the JAL Foundation, and JAMCO Tokyo for supporting the CONTRAIL project. We thank Y. Niwa for providing outputs of NICAM-TM CO_2 simulations. This study was supported by the Green Network of Excellence (GRENE-ei) of the MEXT. This study was performed within the framework of the GOSAT Research Announcement.

References

Araki, M., Morino, I., Machida, T., Sawa, Y., Matsueda, H., Ohyama, H., Yokota, T., and Uchino, O.: CO_2 column-averaged volume mixing ratio derived over Tsukuba from measurements by commercial airlines, Atmos. Chem. Phys., 10, 7659–7667, doi:10.5194/acp-10-7659-2010, 2010.

Bakwin, P. S., Tans, P. P., Hurst, D. F., and Zhao, C.: Measurements of carbon dioxide on very tall towers: results of the NOAA/CMDL program, Tellus B, 50, 401–415, 1998.

AMTD
8, 12993–13037, 2015

Barkley, M. P., Frieß, U., and Monks, P. S.: Measuring atmospheric CO_2 from space using Full Spectral Initiation (FSI) WFM-DOAS, Atmos. Chem. Phys., 6, 3517–3534, doi:10.5194/acp-6-3517-2006, 2006.

Basu, S., Guerlet, S., Butz, A., Houweling, S., Hasekamp, O., Aben, I., Krummel, P., Steele, P., Langenfelds, R., Torn, M., Biraud, S., Stephens, B., Andrews, A., and Worthy, D.: Global CO_2 fluxes estimated from GOSAT retrievals of total column CO_2, Atmos. Chem. Phys., 13, 8695–8717, doi:10.5194/acp-13-8695-2013, 2013.

Basu, S., Krol, M., Butz, A., Clerbaux, C., Sawa, Y., Machida, T., Matsueda, H., Frankenberg, C., Hasekamp, O. P., and Aben, I.: The seasonal variation of the CO_2 flux over Tropical Asia estimated from GOSAT, CONTRAIL, and IASI, Geophys. Res. Lett., 41, 1809–1815, 2014.

Brenninkmeijer, C. A. M., Crutzen, P., Boumard, F., Dauer, T., Dix, B., Ebinghaus, R., Filippi, D., Fischer, H., Franke, H., Frieß, U., Heintzenberg, J., Helleis, F., Hermann, M., Kock, H. H., Koeppel, C., Lelieveld, J., Leuenberger, M., Martinsson, B. G., Miemczyk, S., Moret, H. P., Nguyen, H. N., Nyfeler, P., Oram, D., O'Sullivan, D., Penkett, S., Platt, U., Pupek, M., Ramonet, M., Randa, B., Reichelt, M., Rhee, T. S., Rohwer, J., Rosenfeld, K., Scharffe, D., Schlager, H., Schumann, U., Slemr, F., Sprung, D., Stock, P., Thaler, R., Valentino, F., van Velthoven, P., Waibel, A., Wandel, A., Waschitschek, K., Wiedensohler, A., Xueref-Remy, I., Zahn, A., Zech, U., and Ziereis, H.: Civil Aircraft for the regular investigation of the atmosphere based on an instrumented container: The new CARIBIC system, Atmos. Chem. Phys., 7, 4953–4976, doi:10.5194/acp-7-4953-2007, 2007.

Buchwitz, M., de Beek, R., Burrows, J. P., Bovensmann, H., Warneke, T., Notholt, J., Meirink, J. F., Goede, A. P. H., Bergamaschi, P., Körner, S., Heimann, M., and Schulz, A.: Atmospheric methane and carbon dioxide from SCIAMACHY satellite data: initial comparison with chemistry and transport models, Atmos. Chem. Phys., 5, 941–962, doi:10.5194/acp-5-941-2005, 2005.

Butz, A., Guerlet, S., Hasekamp, O., Schepers, D., Galli, A., Aben, I., Frankenberg, C., Hartmann, J.-M., Tran, H., Kuze, A., Keppel-Aleks, G., Toon, G., Wunch, D., Wennberg, P., Deutscher, N., Griffith, D., Macatangay, R., Messerschmidt, J., Notholt, J., and Warneke, T.: Toward accurate CO_2 and CH_4 observations from GOSAT, Geophys. Res. Lett., 38, L14812, doi:10.1029/2011GL047888, 2011.

Chahine, M., Barnet, C., Olsen, E. T., Chen, L., and Maddy, E.: On the determination of atmospheric minor gases by the method of vanishing partial derivatives with application to CO_2, Geophys. Res. Lett., 32, L22803, doi:10.1029/2005GL024165, 2005.

AMTD
8, 12993–13037, 2015

Chédin, A., Serrar, S., Armante, R., Scott, N. A., and Hollingsworth, A.: Signatures of annual and seasonal variations of CO_2 and other greenhouse gases from comparisons between NOAA TOVS observations and radiation model simulations, J. Climate, 15, 95–116, 2002.
Chédin, A., Serrar, S., Scott, N. A., Crevoisier, C., and Armante, R.: First global measurement of midtropospheric CO_2 from NOAA polar satellites, J. Geophys. Res., 108, 4581, doi:10.1029/2003JD003439, 2003.
Chédin, A., Serrar, S., Scott, N. A., Pierangelo, C., and Ciais, P.: Impact of tropical biomass burning emissions on the diurnal cycle of upper tropospheric CO_2 retrieved from NOAA 10 satellite observations, J. Geophys. Res., 110, D11309, doi:10.1029/2004JD005540, 2005.
Chevallier, F., Fisher, M., Peylin, P., Serrar, S., Bousquet, P., Bréon, F.-M., Chédin, A., and Ciais, P.: Inferring CO_2 sources and sinks from satellite observations: method and application to TOVS data, J. Geophys. Res., 110, D24309, doi:10.1029/2005JD006390, 2005.
Chevallier, F., Palmer, P. I., Feng, L., Boesch, H., O'Dell, C. W., and Bousquet, P.: Toward robust and consistent regional CO_2 flux estimates from in situ and spaceborne measurements of atmospheric CO_2, Geophys. Res. Lett., 41, 1065–1070, 2014.
Climate Modeling and Diagnostics Laboratory (CMDL): Climate Modeling and Diagnostics Laboratory Summary Report No. 27 2002–2003, Boulder, Colorado, USA, 2004.
Cogan, A. J., Boesch, H., Parker, R. J., Feng, L., Palmer, P. I., Blavier, J.-F. L., Deutscher, N. M., Macatangay, R., Notholt, J., Roehl, C., Warneke, T., and Wunch, D.: Atmospheric carbon dioxide retrieved from the Greenhouse gases Observing SATellite (GOSAT): comparison with ground-based TCCON observations and GEOS-Chem model calculations, J. Geophys. Res., 117, D21301, doi:10.1029/2012JD018087, 2012.
Crevoisier, C., Heilliette, S., Chédin, A., Serrar, S., Armante, R., and Scott, N. A.: Midtropospheric CO_2 concentration retrieval from AIRS observations in the tropics, Geophys. Res. Lett., 31, L17106, doi:10.1029/2004GL020141, 2004.
Crevoisier, C., Chédin, A., Matsueda, H., Machida, T., Armante, R., and Scott, N. A.: First year of upper tropospheric integrated content of CO_2 from IASI hyperspectral infrared observations, Atmos. Chem. Phys., 9, 4797–4810, doi:10.5194/acp-9-4797-2009, 2009.
Crevoisier, C., Sweeney, C., Gloor, M., Sarmiento, J. L., and Tans, P. P.: Regional US carbon sinks from three-dimensional atmospheric CO_2 sampling, P. Natl. Acad. Sci. USA, 107, 18348–18353, 2010.
Hamazaki, T., Kaneko, Y., Kuze, A., and Kondo, K.: Fourier transform spectrometer for Greenhouse Gases Observing Satellite (GOSAT), P. Soc. Photo-Opt. Ins., 659, 73–80, 2005.

AMTD
8, 12993–13037, 2015

Imasu, R., Hayashi, Y., Inagoya, A., Saitoh, N., and Shiomi, K.: Retrieval of minor constituents from thermal infrared spectra observed by GOSAT TANSO-FTS sensor, P. Soc. Photo-Opt. Ins., 7857, 785708, doi:10.1117/12.870684, 2010.

Inoue, M., Morino, I., Uchino, O., Miyamoto, Y., Yoshida, Y., Yokota, T., Machida, T., Sawa, Y., Matsueda, H., Sweeney, C., Tans, P. P., Andrews, A. E., Biraud, S. C., Tanaka, T., Kawakami, S., and Patra, P. K.: Validation of XCO_2 derived from SWIR spectra of GOSAT TANSO-FTS with aircraft measurement data, Atmos. Chem. Phys., 13, 9771–9788, doi:10.5194/acp-13-9771-2013, 2013.

Intergovernmental Panel on Climate Change (IPCC): Contribution of Working Group I to the Fifth Assessment Report of the Intergovernmental Panel on Climate Change, Cambridge University Press, Cambridge, UK, New York, NY, USA, 2013.

Ishida, H. and Nakajima, T. Y.: Development of an unbiased cloud detection algorithm for a spaceborne multispectral imager, J. Geophys. Res., 114, D07206, doi:10.1029/2008JD010710, 2009.

Ishida, H., Nakjima, T. Y., Yokota, T., Kikuchi, N., and Watanabe, H.: Investigation of GOSAT TANSO-CAI cloud screening ability through an intersatellite comparison, J. Appl. Meteorol. Clim., 50, 1571–1586, 2011.

Karion, A., Sweeney, C., and Tans, P. P.: AirCore: an innovative atmospheric sampling system, J. Atmos. Ocean. Tech., 27, 1839–1853, 2010.

Kataoka, F., Knuteson, R. O., Kuze, A., Suto, H., Shiomi, K., Harada, M., Garms, E. M., Roman, J. A., Tobin, D. C., Taylor, J. K., Revercomb, H. E., Sekio, N., Higuchi, R., and Mitomi, Y.: TIR spectral radiance calibration of the GOSAT satellite borne TANSO-FTS with the aircraft-based S-HIS and the ground-based S-AERI at the Railroad Valley desert playa, IEEE T. Geosci. Remote, 52, 89–105, 2014.

Keeling, C. D., Bacastow, R. B., Bainbridge, A. E., Ekdahl, C. A., Guenther, P. R., Waterman, L. S., and Chin, J. F. S.: Atmospheric carbon dioxide variations at Mauna Loa Observatory, Hawaii, Tellus, 28, 538–551, 1976a.

Keeling, C. D., Adams, J. A., Ekdahl, C. A., and Guenther, P. R.: Atmospheric carbon dioxide variations at the South Pole, Tellus, 28, 553–564, 1976b.

Keeling, C. D., Chin, J. F. S., and Whorf, T. P.: Increased activity of northern vegetation inferred from atmospheric CO_2 measurements, Nature, 382, 146–149, 1996.

Kulawik, S. S., Jones, D. B. A., Nassar, R., Irion, F. W., Worden, J. R., Bowman, K. W., Machida, T., Matsueda, H., Sawa, Y., Biraud, S. C., Fischer, M. L., and Jacobson, A. R.:

AMTD
8, 12993–13037, 2015

Characterization of Tropospheric Emission Spectrometer (TES) CO_2 for carbon cycle science, Atmos. Chem. Phys., 10, 5601–5623, doi:10.5194/acp-10-5601-2010, 2010.

Kulawik, S. S., Worden, J. R., Wofsy, S. C., Biraud, S. C., Nassar, R., Jones, D. B. A., Olsen, E. T., Jimenez, R., Park, S., Santoni, G. W., Daube, B. C., Pittman, J. V., Stephens, B. B., Kort, E. A., Osterman, G. B., and TES team: Comparison of improved Aura Tropospheric Emission Spectrometer CO_2 with HIPPO and SGP aircraft profile measurements, Atmos. Chem. Phys., 13, 3205–3225, doi:10.5194/acp-13-3205-2013, 2013.

Kuze, A., Suto, H., Nakajima, M., and Hamazaki, T.: Thermal and near infrared sensor for carbon observation Fourier-transform spectrometer on the Greenhouse Gases Observing Satellite for greenhouse gases monitoring, Appl. Optics, 48, 6716–6733, 2009.

Kuze, A., Suto, H., Shiomi, K., Urabe, T., Nakajima, M., Yoshida, J., Kawashima, T., Yamamoto, Y., Kataoka, F., and Buijs, H.: Level 1 algorithms for TANSO on GOSAT: processing and on-orbit calibrations, Atmos. Meas. Tech., 5, 2447–2467, doi:10.5194/amt-5-2447-2012, 2012.

Machida, T., Matsueda, H., Sawa, Y., Nakagawa, Y., Hirotani, K., Kondo, N., Goto, K., Nakazawa, T., Ishikawa, K., and Ogawa, T.: Worldwide measurements of atmospheric CO_2 and other trace gas species using commercial airlines, J. Atmos. Ocean. Tech., 25, 1744–1754, 2008.

Machida, T., Tohjima, Y., Katsumata, K., and Mukai, H.: A new CO_2 calibration scale based on gravimetric one-step dilution cylinders in National Institute for Environmental Studies – NIES 09 CO_2 Scale, 15th WMO/IAEA Meeting of Experts on Carbon Dioxide, Other Greenhouse Gases and Related Tracers Measurement Techniques, GAW Rep., 194, World Meteorological Organization, Geneva, Switzerland, 165–169, 2011.

Maddy, E. S., Barnet, C. D., Goldberg, M., Sweeney, C., and Liu, X.: CO_2 retrievals from the Atmospheric Infrared Sounder: methodology and validation, J. Geophys. Res., 113, doi:10.1029/2007JD009402, 2008.

Maksyutov, S., Takagi, H., Valsala, V. K., Saito, M., Oda, T., Saeki, T., Belikov, D. A., Saito, R., Ito, A., Yoshida, Y., Morino, I., Uchino, O., Andres, R. J., and Yokota, T.: Regional CO_2 flux estimates for 2009–2010 based on GOSAT and ground-based CO_2 observations, Atmos. Chem. Phys., 13, 9351–9373, doi:10.5194/acp-13-9351-2013, 2013.

Matsueda, H., Machida, T., Sawa, Y., Nakagawa, Y., Hirotani, K., Ikeda, H., Kondo, N., and Goto, K.: Evaluation of atmospheric CO_2 measurements from new flask air sampling of JAL airliner observations, Pap. Meteorol. Geophys., 59, 1–17, 2008.

AMTD
8, 12993–13037, 2015

Matsueda, H., Machida, T., Sawa, Y., and Niwa, Y.: Long-term change of CO_2 latitudinal distribution in the upper troposphere, Geophys. Res. Lett., 42, 2508–2514, 2015.

McPeters, R. D., Labow, G. J., and Logan, J. A.: Ozone climatological profiles for satellite retrieval algorithms, J. Geophys. Res., 112, D05308, doi:10.1029/2005JD006823, 2007.

Nassar, R., Jones, D. B. A., Kulawik, S. S., Worden, J. R., Bowman, K. W., Andres, R. J., Suntharalingam, P., Chen, J. M., Brenninkmeijer, C. A. M., Schuck, T. J., Conway, T. J., and Worthy, D. E.: Inverse modeling of CO_2 sources and sinks using satellite observations of CO_2 from TES and surface flask measurements, Atmos. Chem. Phys., 11, 6029–6047, doi:10.5194/acp-11-6029-2011, 2011.

Niwa, Y., Tomita, H., Satoh, M., and Imasu, R.: A threedimensional icosahedral grid advection scheme preserving monotonicity and consistency with continuity for atmospheric tracer transport, J. Meteorol. Soc. Jpn., 89, 255–268, 2011.

Niwa, Y., Machida, T., Sawa, Y., Matsueda, H., Schuck, T. J., Brenninkmeijer, C. A. M., Imasu, R., and Satoh, M.: Imposing strong constraints on tropical terrestrial CO_2 fluxes using passenger aircraft based measurements, J. Geophys. Res., 117, D11303, doi:10.1029/2012JD017474, 2012.

O'Dell, C. W., Connor, B., Bösch, H., O'Brien, D., Frankenberg, C., Castano, R., Christi, M., Eldering, D., Fisher, B., Gunson, M., McDuffie, J., Miller, C. E., Natraj, V., Oyafuso, F., Polonsky, I., Smyth, M., Taylor, T., Toon, G. C., Wennberg, P. O., and Wunch, D.: The ACOS CO_2 retrieval algorithm – Part 1: Description and validation against synthetic observations, Atmos. Meas. Tech., 5, 99–121, doi:10.5194/amt-5-99-2012, 2012.

Ohyama, H., Kawakami, S., Shiomi, K., and Miyagawa, K.: Retrievals of total and tropospheric ozone from GOSAT thermal infrared spectral radiances, IEEE T. Geosci. Remote, 50, 1770–1784, 2012.

Ohyama, H., Kawakami, S., Shiomi, K., Morino, I., and Uchino, O.: Atmospheric temperature and water vapor retrievals from GOSAT thermal infrared spectra and initial validation with coincident radiosonde measurements, SOLA, 9, 143–147, 2013.

Pak, B. C. and Prather, M. J.: CO_2 sources inversions using satellite observations of the upper troposphere, Geophys. Res. Lett., 28, 4571–4574, 2001.

Rayner, P. J. and O'Brien, D. M.: The utility of remotely sensed CO_2 concentration data in surface source inversions, Geophys. Res. Lett., 28, 175–178, 2001.

Rodgers, C. D.: Inverse Method for Atmospheric Sounding, World Scientific Publishing, Singapore, 2000.

AMTD
8, 12993–13037, 2015

Rodgers, C. D. and Connor, B. J.: Intercomparison of remote sounding instruments, J. Geophys. Res., 108, 4116, doi:10.1029/2002JD002299, 2003.

Saeki, T., Maksyutov, S., Saito, M., Valsala, V., Oda, T., Andres, R. J., Belikov, D., Tans, P., Dlugokencky, E., Yoshida, Y., Morino, I., Uchino, O., and Yokota, T.: Inverse modeling of CO_2 fluxes using GOSAT data and multi-year ground-based observations, SOLA, 9, 45–50, 2013a.

Saeki, T., Saito, R., Belikov, D., and Maksyutov, S.: Global high-resolution simulations of CO_2 and CH_4 using a NIES transport model to produce a priori concentrations for use in satellite data retrievals, Geosci. Model Dev., 6, 81–100, doi:10.5194/gmd-6-81-2013, 2013b.

Saitoh, N., Imasu, R., Ota, Y., and Niwa, Y.: CO_2 retrieval algorithm for the thermal infrared spectra of the Greenhouse Gases Observing Satellite: potential of retrieving CO_2 vertical profile from high-resolution FTS sensor, J. Geophys. Res., 114, D17305, doi:10.1029/2008JD011500, 2009.

Saitoh, N., Touno, M., Hayashida, S., Imasu, R., Shiomi, K., Yokota, T., Yoshida, Y., Machida, T., Matsueda, H., and Sawa, Y.: Comparisons between XCH_4 from GOSAT Shortwave and Thermal Infrared Spectra and Aircraft CH_4 Measurements over Guam, SOLA, 8, 145–149, 2012.

Sawa, Y., Machida, T., and Matsueda, H.: Aircraft observation of the seasonal variation in the transport of CO_2 in the upper atmosphere, J. Geophys. Res., 117, D05305, doi:10.1029/2011JD016933, 2012.

Strow, L. L. and Hannon, S. E.: A 4-year zonal climatology of lower tropospheric CO_2 derived from ocean-only atmospheric infrared sounder observations, J. Geophys. Res., 113, D18302, doi:10.1029/2007JD009713, 2008.

Takagi, H., Houweling, S., Andres, R. J., Belikov, D., Bril, A., Boesch, H., Butz, A., Guerlet, S., Hasekamp, O., Maksyutov, S., Morino, I., Oda, T., O'Dell, C. W., Oshchepkov, S., Parker, R., Saito, M., Uchino, O., Yokota, T., Yoshida, Y., and Valsala, V.: Influence of differences in current GOSAT XCO_2 retrievals on surface flux estimation, Geophys. Res. Lett., 41, 2598–2605, 2014.

Yokota, T., Yoshida, Y., Eguchi, N., Ota, Y., Tanaka, T., Watanabe, H., and Maksyutov, S.: Global concentrations of CO_2 and CH_4 retrieved from GOSAT: first preliminary results, SOLA, 5, 160–163, 2009.

Yoshida, Y., Ota, Y., Eguchi, N., Kikuchi, N., Nobuta, K., Tran, H., Morino, I., and Yokota, T.: Retrieval algorithm for CO_2 and CH_4 column abundances from short-wavelength infrared

AMTD
8, 12993–13037, 2015

spectral observations by the Greenhouse gases observing satellite, Atmos. Meas. Tech., 4, 717–734, doi:10.5194/amt-4-717-2011, 2011.

Yoshida, Y., Kikuchi, N., Morino, I., Uchino, O., Oshchepkov, S., Bril, A., Saeki, T., Schutgens, N., Toon, G. C., Wunch, D., Roehl, C. M., Wennberg, P. O., Griffith, D. W. T., Deutscher, N. M., Warneke, T., Notholt, J., Robinson, J., Sherlock, V., Connor, B., Rettinger, M., Sussmann, R., Ahonen, P., Heikkinen, P., Kyrö, E., Mendonca, J., Strong, K., Hase, F., Dohe, S., and Yokota, T.: Improvement of the retrieval algorithm for GOSAT SWIR XCO_2 and XCH_4 and their validation using TCCON data, Atmos. Meas. Tech., 6, 1533–1547, doi:10.5194/amt-6-1533-2013, 2013.

AMTD
8, 12993–13037, 2015

Table 1. Retrieval grid layers of GOSAT/TANSO-FTS TIR CO_2 V1.0 data.

Layer level	Lower presure level (hPa)	Upper pressure level (hPa)
1	1165.91	857.70
2	857.70	735.64
3	735.64	630.96
4	630.96	541.17
5	541.17	464.16
6	464.16	398.11
7	398.11	341.45
8	341.45	287.30
9	287.30	237.14
10	237.14	195.73
11	195.73	161.56
12	161.56	133.35
13	133.35	110.07
14	110.07	90.85
15	90.85	74.99
16	74.99	61.90
17	61.90	51.09
18	51.09	42.17
19	42.17	34.81
20	34.81	28.73
21	28.73	23.71
22	23.71	19.57
23	19.57	16.16
24	16.16	13.34
25	13.34	10.00
26	10.00	5.62
27	5.62	1.00
28	1.00	0.10

AMTD
8, 12993–13037, 2015

Table 2. Bias values of GOSAT/TANSO-FTS TIR V1.0 CO_2 data against CONTRAIL CME CO_2 data for each season and each latitude region in the upper troposphere and lower stratosphere in the unit of ppm. Significant bias values larger than ±1.0 ppm are indicated by boldface. The evaluation of the bias values does not consider TIR CO_2 averaging kernel functions.

UT LS	MAM		JJA		SON		JF (DJF)	
60–70° N	−0.8	0.3	0.2	−0.3	−0.6	**−2.0**	0.3	−0.1
40–60° N	**−2.2**	**1.2**	**−1.2**	**−1.2**	−0.7	**−1.0**	0.2	−0.4
20–40° N	**−2.7**		**−1.6**		−0.4		0.2	
0–20° N	−0.8		**−2.0**		−0.2		0.8	
20° S–0	0.3		−0.2		0.5		0.4	
40–20° S	0.5		−0.1		−0.5		0.1	

AMTD
8, 12993–13037, 2015

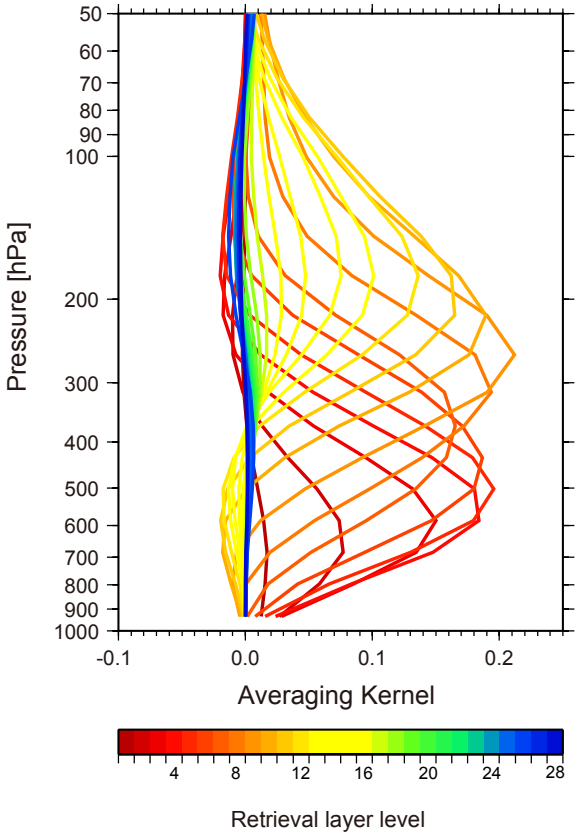

Figure 1. Averaging kernel functions of GOSAT/TANSO-FTS TIR V1.0 CO_2 retrieval in the 28 retrieval grid layers shown in Table 1.

AMTD
8, 12993–13037, 2015

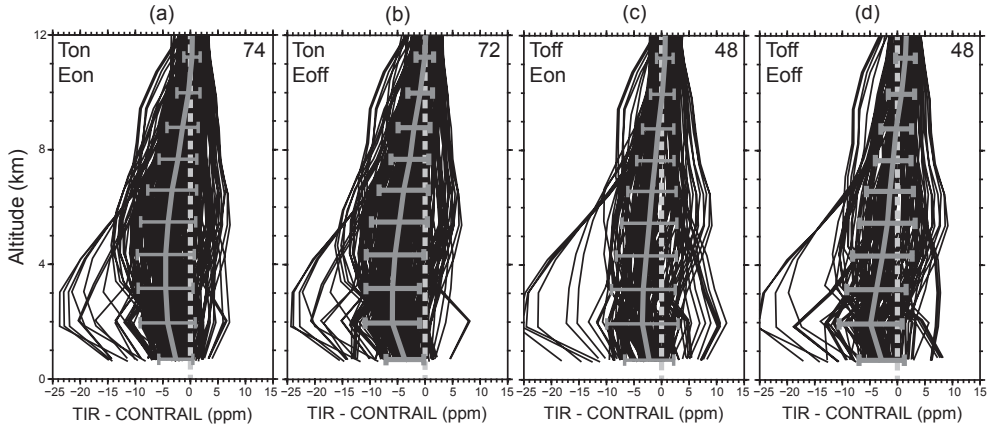

Figure 2. Differences between GOSAT/TANSO-FTS TIR retrieved CO_2 profiles and the corresponding CONTRAIL CME ascending/descending data over Narita airport with considering TIR CO_2 averaging kernel functions. Thin black lines show individual comparisons. Thick gray lines and horizontal bars show the means and 1-σ standard deviations of the comparisons. The upper right number of each panel indicates the number of all of the GOSAT/TANSO-FTS TIR CO_2 profiles among the 141 pairs that were normally retrieved under each retrieval condition: **(a)** Ton & Eon, **(b)** Ton & Eoff, **(c)** Toff & Eon, and **(d)** Toff & Eoff. See the text for details of the retrieval conditions.

AMTD
8, 12993–13037, 2015

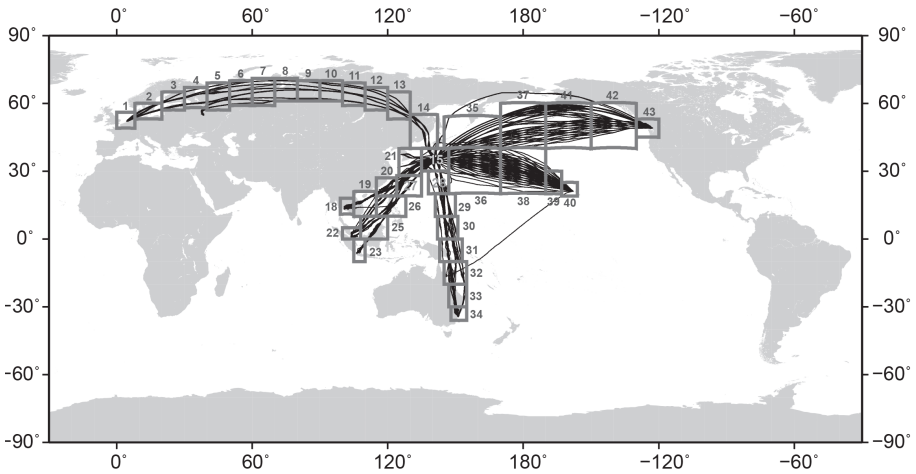

Figure 3. Flight tracks of all of the CONTRAIL CME observations in 2010 used in this study. A number next to a box area indicates each area number.

AMTD
8, 12993–13037, 2015

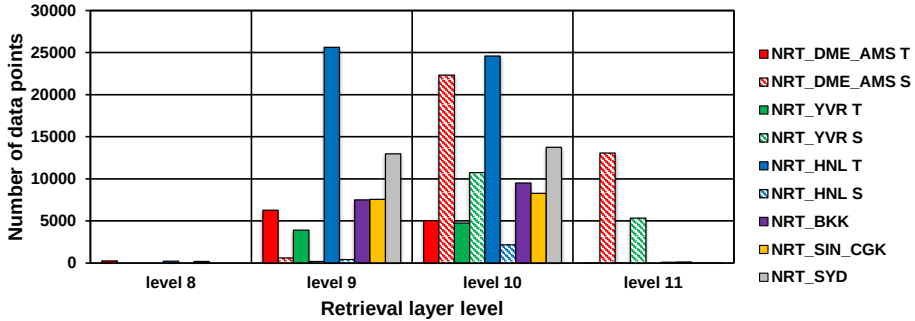

Figure 4. The number of GOSAT/TANSO-FTS TIR CO_2 data points compared to the CONTRAIL CME level flight data for each retrieval grid layer level for each flight. The numbers of TIR CO_2 data points in the troposphere ("T") and stratosphere ("S") are shown separately for the Tokyo–Europe (NRT_DME_AMS), Tokyo–Vancouver (NRT_YVR), and Tokyo–Honolulu (NRT_HNL) flight routes.

AMTD
8, 12993–13037, 2015

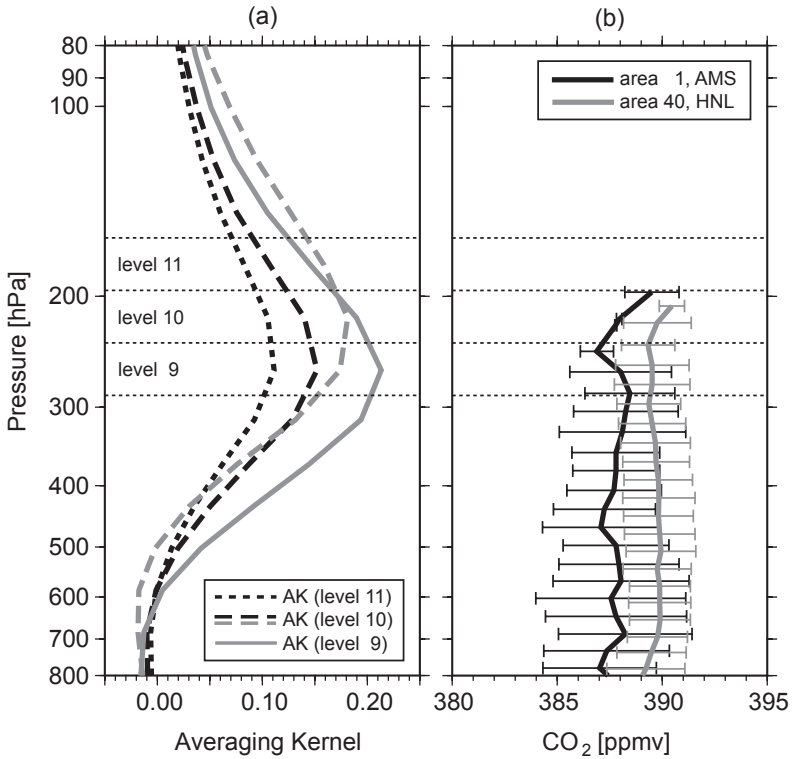

Figure 5. (a) Averaging kernel function of each of the three layer levels 9, 10, and 11, shown by solid, dashed, and dotted lines, respectively. Black and gray lines show the means of averaging kernel functions of all of the GOSAT/TANSO-FTS TIR CO_2 profiles used in the comparisons made in areas 1 and 40 in summer (JJA), respectively. **(b)** Mean profiles with 1-σ standard deviations of CONTRAIL CME ascending/descending CO_2 data over Amsterdam (located in area 1) and Honolulu (located in area 40) airports in summer (JJA), shown by black and gray lines, respectively.

AMTD
8, 12993–13037, 2015

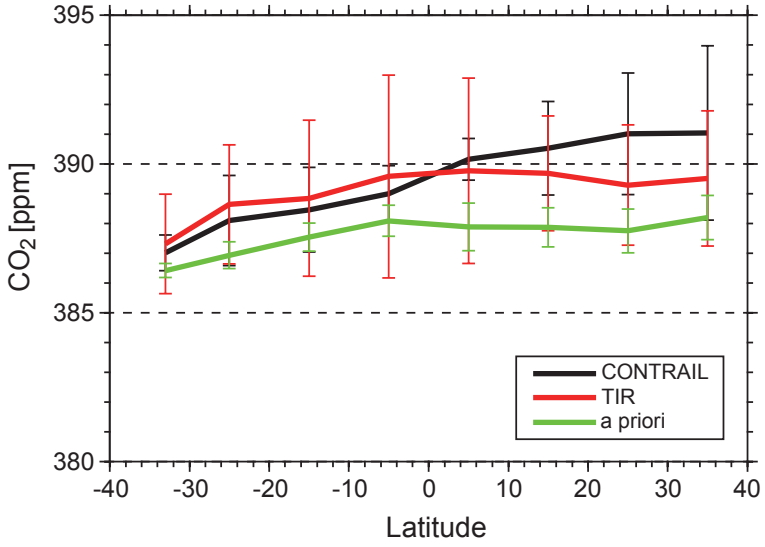

Figure 6. Comparisons among CONTRAIL CME level flight, GOSAT/TANSO-FTS TIR, and a priori (NIES TM 05) CO_2 data during flights between Tokyo and Sydney (NRT_SYD) in spring (MAM), shown by black, red, and green lines, respectively. The means and their 1-σ standard deviations were calculated in each area during the flight for all three datasets.

AMTD
8, 12993–13037, 2015

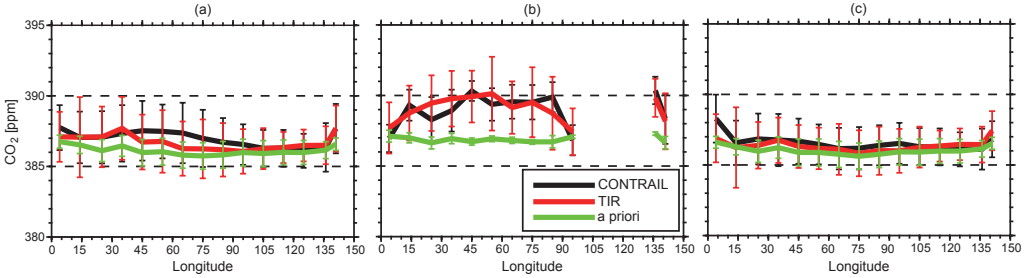

Figure 7. Same as Fig. 6, but for flights between Tokyo and Europe (NRT_DME_AMS) in winter (JF). **(a)** All of the data, **(b)** only data in the troposphere, and **(c)** only data in the stratosphere. See the text for the classification of tropospheric and stratospheric data.

AMTD
8, 12993–13037, 2015

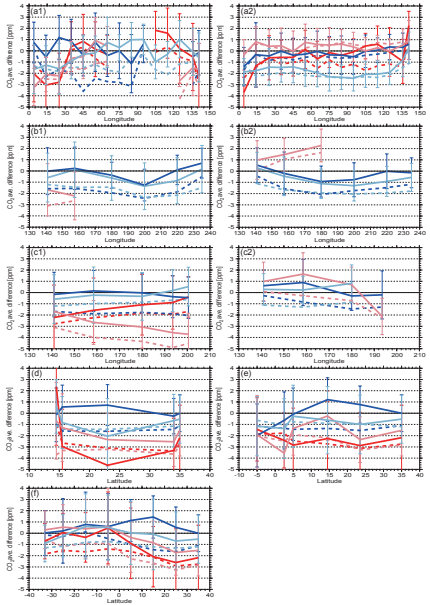

Figure 8. Differences between GOSAT/TANSO-FTS TIR and CONTRAIL CME averaged CO_2 data (TIR ave. minus CONTRAIL ave.) and a priori (NIES TM 05) and CONTRAIL CME averaged CO_2 data (a priori ave. minus CONTRAIL ave.) for each season and each area of all of the six flight routes, shown by thick and dashed lines, respectively: **(a)** Tokyo–Europe (NRT_DME_AMS), **(b)** Tokyo–Vancouver (NRT_YVR), **(c)** Tokyo–Honolulu (NRT_HNL), **(d)** Tokyo–Bangkok (NRT_BKK), **(e)** Tokyo–East Asia (NRT_SIN_CGK), and **(f)** Tokyo–Sydney (NRT_SYD). The means of the differences were calculated for each of the areas in spring (MAM), summer (JJA), fall (SON), and winter (JF/DJF), as shown by the pink, red, light blue, and blue lines, respectively. The 1-σ standard deviations of the averages of TANSO-FTS TIR CO2 data are shown by vertical bars. For the airline routes of Tokyo–Europe, Tokyo–Vancouver, and Tokyo–Honolulu, the results only for the tropospheric data (a1, b1, and c1) and only for the stratospheric data (a2, b2, and c2) are shown separately. Data in December 2010 were used only in the comparisons for the flight between Tokyo and Vancouver.

AMTD
8, 12993–13037, 2015

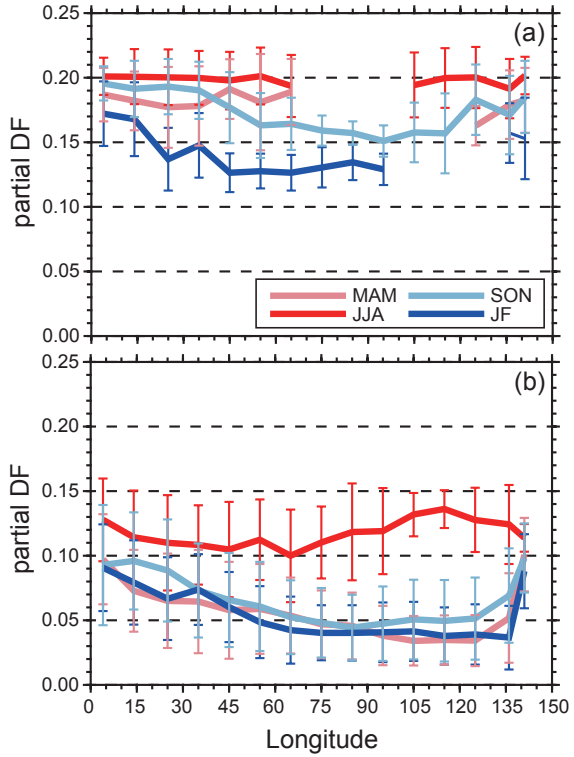

Figure 9. Partial degree of freedom (DF) for GOSAT/TANSO-FTS TIR CO_2 data in the upper troposphere **(a)** and the lower stratosphere **(b)** for each area of the flight between Tokyo and Europe (NRT_DME_AMS). The means and their 1-σ standard deviations of the partial DF data were calculated in spring (MAM), summer (JJA), fall (SON), and winter (JF), as shown by the pink, red, light blue, and blue lines, respectively.

AMTD
8, 12993–13037, 2015

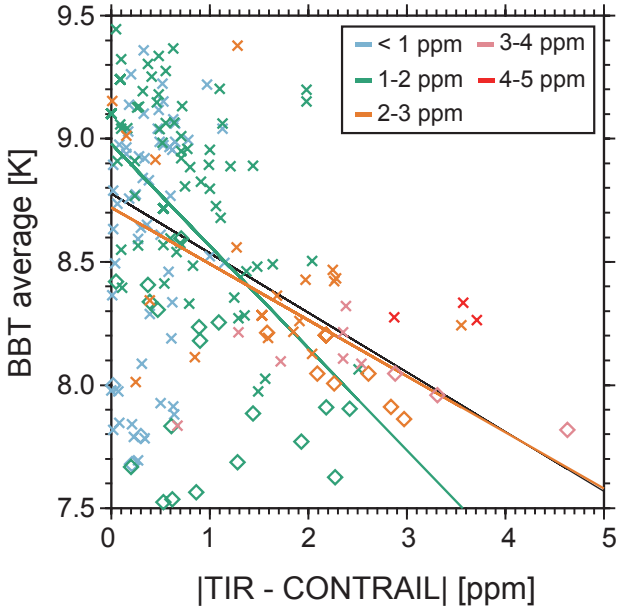

Figure 10. Correlations between the mean temperatures of the internal blackbody (BBT) on board the GOSAT/TANSO-FTS instrument and the differences between GOSAT/TANSO-FTS TIR and CONTRAIL CME averaged CO_2 data (TIR ave. minus CONTRAIL ave.) for each area of all flights for each of the four seasons. All of the data are categorized according to the differences between corresponding a priori (NIES TM 05) and CONTRAIL CME averaged CO_2 data (a priori ave. minus CONTRAIL ave.): less than 1 ppm (light blue), 1–2 ppm (green), 2–3 ppm (orange), 3–4 ppm (pink), and 4–5 ppm (red). Regression lines of the "1–2 ppm" dataset, the "2–3 ppm" dataset and all of the datasets are shown by green, orange, and black lines, respectively. The correlation coefficients of the green, orange, and black lines are −0.49, −0.56, and −0.41, respectively.

AMTD
8, 12993–13037, 2015